

Cite this: *Mater. Adv.*, 2025,
6, 6493

Efficacy of PVX and PEGylated PVX as intratumoral immunotherapy

Yifeng Ma,^{abcd} Mary G. Gorman,^{ab} Juliane Schuphanⁱ and
Nicole F. Steinmetz^{id} *^{abcdeh}

Intratumoral immunotherapy harnesses the tumor microenvironment to enhance local immune activation and systemic antitumor responses. Plant virus nanoparticles have emerged as potent immunostimulatory agents for this strategy. Here, we investigate the efficacy of PEGylated potato virus X (PVX-PEG) in a B-cell lymphoma model. We synthesized PVX-PEG using bis-PEG_n-NHS esters and confirmed successful conjugation through SDS-PAGE, dynamic light scattering, and transmission electron microscopy. PEGylation improved formulation stability, as evidenced by increased thermal resistance and reduced aggregation in biological conditions. *In vivo*, PVX-PEG exhibited prolonged tumor retention and maintained its immunotherapeutic efficacy, comparable to native PVX. Furthermore, antibody recognition of PVX-PEG was significantly reduced, highlighting its potential for clinical translation. These results suggest that PVX-PEG retains the immunostimulatory benefits of PVX while overcoming key formulation and immunogenicity challenges, supporting its advancement as a novel intratumoral immunotherapy for lymphoma.

Received 10th March 2025,
Accepted 30th July 2025

DOI: 10.1039/d5ma00215j

rsc.li/materials-advances

Introduction

Cancer immunotherapy has revolutionized oncology by harnessing the immune system to target and eliminate malignant cells. However, systemic immunotherapy approaches, such as immune checkpoint inhibitors (ICIs), chimeric antigen receptor (CAR) T cells, and cytokine therapies, often face challenges related to immune-related adverse events (irAEs), limited tumor penetration, and immune suppression within the tumor microenvironment (TME).¹ Intratumoral immunotherapy has emerged as a promising alternative where the immunotherapeutic agents are directly injected into a tumor, bypassing

systemic circulation to enhance local immune responses. This strategy can modulate the TME, recruit and activate antigen-presenting cells, and induce systemic antitumor immunity through the abscopal effect, in which immune responses extend beyond the treated lesion to distant metastases.^{2–4} By leveraging the tumor as the source of antigen, intratumoral immunotherapy enhances tumor antigen presentation and T cell priming, overcoming key resistance mechanisms encountered in systemic approaches.

A diverse range of intratumoral immunotherapy approaches are currently under investigation, including Toll-like receptor (TLR) agonists, oncolytic viruses, cytokines, and gene-modified immune cells.^{2–4} Our approach centers on the application of plant viruses for intratumoral immunotherapy. Unlike oncolytic viruses, plant viruses do not target or lyse cancer cells – instead, the plant viral nucleoprotein components act as immunomodulators activating and recruiting innate immune cells to the TME. While plant viruses are non-infectious toward mammals, their repetitive coat proteins and single-stranded RNA cargos stimulate the immune systems through pattern recognition receptors, specifically toll-like receptors (TLRs).^{5,6} For example, we demonstrated that cowpea mosaic virus (CPMV) upon intratumoral injection stimulates a potent anti-tumor immune response in tumor mouse models,⁷ and more importantly in companion canine cancer patients.⁸ When compared to other icosahedral plant viruses, CPMV appears to have a unique anti-tumor potency.^{7,9} However, we and others also reported anti-tumor efficacy of intratumorally applied

^a Aiiso Yufeng Li Family Department of Chemical and Nano Engineering, University of California, San Diego La Jolla, CA 92093, USA. E-mail: nsteinmetz@ucsd.edu

^b Shu and K.C. Chien and Peter Farrell Collaboratory, University of California, San Diego La Jolla, CA 92093, USA

^c Center for Nano-ImmunoEngineering, University of California, San Diego La Jolla, CA 92093, USA

^d Moores Cancer Center, University of California, San Diego La Jolla, CA 92093, USA

^e Department of Bioengineering, University of California, San Diego La Jolla, CA 92093, USA

^f Department of Radiology, University of California, San Diego La Jolla, CA 92093, USA

^g Institute for Materials Discovery and Design, University of California, San Diego La Jolla, CA 92093, USA

^h Center for Engineering in Cancer, Institute of Engineering Medicine, University of California, San Diego La Jolla, CA 92093, USA

ⁱ Institut für Molekulare Biotechnologie, RWTH Aachen University, Worringer Weg 1, 52074 Aachen, Germany



filamentous plant viruses such as papaya mosaic virus (PapMV)¹⁰ and potato virus (PVX).¹¹

In a recent study we tested activity of PVX against non-Hodgkin's lymphoma (NHL) in a mouse model. While intratumoral immunotherapy has focused on solid tumors, there is a rationale for applying this strategy to NHL, as patients often present with injectable lesions, making *in situ* treatment an attainable option.^{12,13} In fact, recent developments using small molecule TLR agonists as well as intratumoral cytokines (*e.g.*, Flt3L) highlight the opportunity for intratumoral immunotherapy for lymphoma^{12–14} [NCT01976585]. Our study demonstrated efficacy of PVX against B-cell lymphoma (A20 and BALB/C mice). PVX elicited systemic and long-lasting anti-tumor efficacy, preventing the recurrence of A20 lymphoma in rechallenge experiments. Mechanistic insights indicated that

myeloid cells (neutrophils) were the primary responders leading to antigen processing and adaptive anti-tumor immunity.¹¹

PVX possess a filamentous structure (515 × 13 nm) which is challenging to replicate synthetically – however the filamentous morphology may be advantageous for tissue penetration, cell interactions and cargo loading, *e.g.* combination with mRNA therapeutics or small molecules or biologics. To begin the development of PVX as a platform for intratumoral immunotherapy applications, we set out to test the anti-tumor efficacy of a PEGylated PVX. The rationale for testing PVX-PEG is supported by several studies that indicated human exposure and pre-existing immunity against various plant viruses.^{15–17} Thus the application of native PVX as a biologic may result in premature antibody-mediated clearance or off-target effects such as complement activation-related

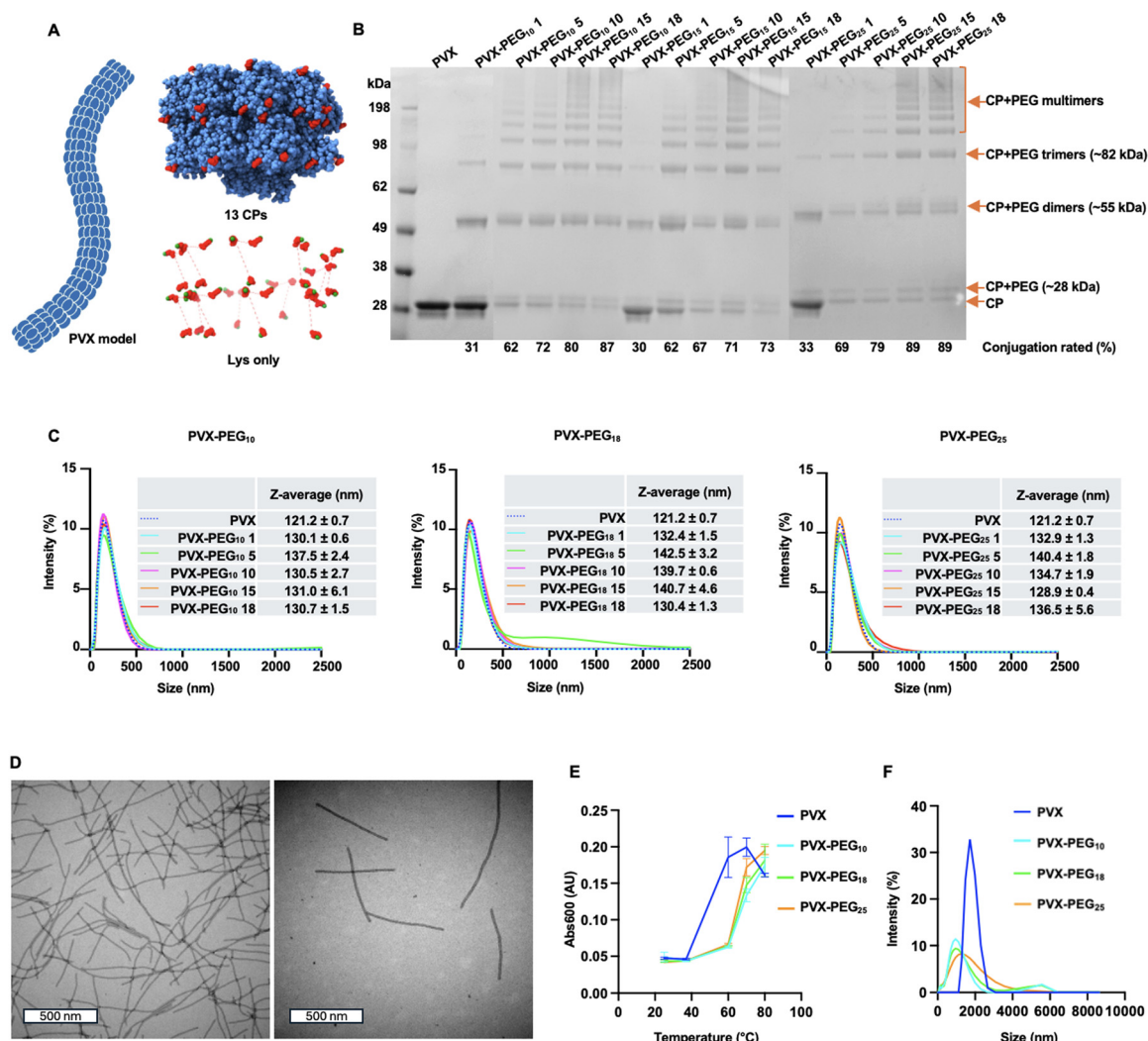


Fig. 1 Synthesis and characterization of PVX-PEG_n. (A) Schematic representation of the structure of PVX (left) and 13 coat protein (CP) units highlighting solvent exposed lysine residues (Lys 61, Lys 70, and Lys 177) labelled in red; the primary amine groups are labelled in green; the structure was analyzed using UCSF ChimeraX software and Protein Data Bank entry 6R7G (right). (B) SDS-PAGE gel and (C) DLS analyzing PVX and crosslinked PVX-PEG_n ($n = 10, 18, 25$) at different molar ratio of CP and PEG_n. The conjugation rate was calculated with Fiji ImageJ band analysis tool. (D) TEM of negatively stained PVX (left) and crosslinked PVX-PEG_n (right). (E) Turbidimetric assay (absorbance at 600 nm) to determine aggregation rate of PVX and crosslinked PVX-PEG_n heated from 25 to 80 °C for 15 min. (F) DLS of PVX and crosslinked PVX-PEG_n heated at 60 °C for 15 min.



pseudoallergy (CARPA).¹⁸ PEGylation is often applied to biologics for example several PEGylated cytokine therapies and vaccines have been tested for intratumoral administration. PEGylation improves pharmacodynamic and pharmacokinetics properties of biologics.¹⁹

In the present work, we used a bioconjugation method and two-arm PEG chains to produce crosslinked PVX-PEG – this strategy was chosen, because in previous work we had shown that the increased surface coverage with PEG that is interlinking PVX coat proteins is most efficient to enhance the pharmacology and reduce antibody recognition of PVX, as opposed to conjugation or linear PEG arms anchored to a single coat protein.²⁰ PVX-PEG was produced and its efficacy evaluated using a murine model of B cell lymphoma.

Results & discussion

Synthesis and characterization of PVX-PEG

PVX features multiple chemically reactive lysine and cysteine residues on its external surface.²¹ Structural analysis highlights – while cysteine residues are relatively more buried – several lysine side chains are solvent exposed. Fig. 1A shows 13 coat protein (CP) units of the PVX virion, corresponding to 1.5 helical turns. The solvent-exposed lysine residues Lys 61, Lys 70, and Lys 177 are highlighted in red. The distances between the primary amine groups (shown in green) on adjacent CP units range from 10.8 Å to 63.5 Å. Given the structural data, we chose bivalent linear bis-PEG_n-NHS esters with $n = 10, 18,$ and 25 with contour lengths of 27.8 Å, 50.0 Å and 69.5 Å, respectively (calculated as $n \times 2.78 \text{ \AA}$).²² While PEG chains in solution adapt ‘mushroom-like’ rather than linear conformations, we selected these PEG chain lengths to test PEGylation and crosslinking efficiency. At least in theory, these PEG chains could react with adjacent CPs within the same PVX particle. The bis-PEG_n-NHS esters were reacted with PVX using PEG linkers at various ratios per CP (1:1, 5:1, 10:1, 15:1, and 18:1).

Denaturing SDS-PAGE was used to analyze the degree of PEG chain conjugation and CP crosslinking (Fig. 1B). PEG conjugation was evident by appearance of higher molecular weight (M_w) bands; conjugation of a single PEG $n = 10$ chain would result in an MW increase of the CP by ~ 500 Da, conjugation of PEG $n = 18$ or $n = 25$ in a MW increase of 900 or 1250 Da. Indeed, conjugation was apparent, and the conjugation degree increased with increasing molecular excess used, as expected. If crosslinking occurs, CP dimers are expected, and dimerization is detected independent of the chain length used. Of note, trimers and higher-order multimers were also observed for all formulations tested. While the bivalent PEG chains can only conjugate to two lysines, the multiple band pattern and heterogeneity can be explained by the multiple solvent-exposed and reactive lysine residues on the PVX coat proteins that are conjugated with PEG molecules – this likely will result in entanglement of the CP-PEG complexes. Intraparticle rather than interparticle crosslinking is expected given the use of rather short, low molecular weight PEGs and

our previous investigation.²⁰ DLS was used to characterize the crosslinked PVX-PEG_n formulations. Of note, while DLS is less effective in providing accurate size measurements for high aspect ratio particles such as PVX, it remains valuable for identifying trends in particle behavior. Specifically, DLS can provide insights of aggregation, particle breakage, or changes in size distribution of filamentous nanoparticles. DLS measurements were consistent with intraparticle crosslinking – the hydrodynamic diameter of the PVX-PEG_n increased as a function of PEG_n conjugation, but overall narrow size distribution comparable to that of native PVX was noted (Fig. 1C). This is consistent with PEG conjugation and intraparticle crosslinking – because interparticle crosslinking would result in size increases and given the high degree of multivalency, likely in extensive aggregation, which was not observed. Finally, TEM imaging showed intact PVX-PEG matching the appearance of native PVX (Fig. 1D).

Formulation stability of PVX-PEG is increased

To gain insights into the formulation stability, we conducted thermal stability assays. First, PVX and PVX-PEG_n in potassium phosphate buffer were heated from 25 °C to 80 °C over 15 min and stability was assayed as a function of turbidimetry measurement by reading absorbance at Abs₆₀₀ readout (Fig. 1E). Data indicate increased stability of PVX-PEG_n; while native PVX begins to aggregate when temperature exceeds 40 °C, changes in Abs₆₀₀ are not apparent until PVX-PEG_n reached 60 °C. There were no apparent differences comparing PVX conjugated with PEG₁₀, PEG₁₈, and PEG₂₅. Data align with literature reports showing that the PVX coat protein begins to aggregate when incubated at temperatures above 35 °C.¹⁵ Thus, the turbidimetric assay indicates that PEG crosslinking improves the thermal stability of PVX from 40 °C to 60 °C. DLS measurement correlates with the turbidimetric assay. When PVX or PVX-PEG_n was incubated at 60 °C – DLS measurement indicates that PVX-PEG_n remained stable, while native PVX formed aggregates (Fig. 1F).

Finally, we conducted preliminary assays to test stability under physiological conditions by exposing PVX and PVX-PEG_n to mouse serum and incubated samples for 24 hours at 37 °C. Visual inspection (data not shown; we attempted to capture the aggregation in photographs but due to the lack of contrast this was challenging) indicated that samples of PVX appeared in an opaque color indicative of protein aggregation and precipitation. PVX-PEG_n samples remained clear indicating sample stability in biological media.

PEGylated PVX maintains its anti-tumor efficacy

To evaluate the anti-tumor immunotherapeutic efficacy of PVX vs. the PVX-PEG, we used a murine lymphoma tumor model by implanting A20 cells intradermally into the right flank of BALB/c mice. There was no significant difference in the formulation properties comparing PVX conjugated with PEG₁₀, PEG₁₈, or PEG₂₅; PVX-PEG₁₀ was selected for *in vivo* studies. Once the tumor volume reached approximately 30 mm³, A20 tumor-bearing mice were treated with PBS, PVX, or PVX-PEG₁₀



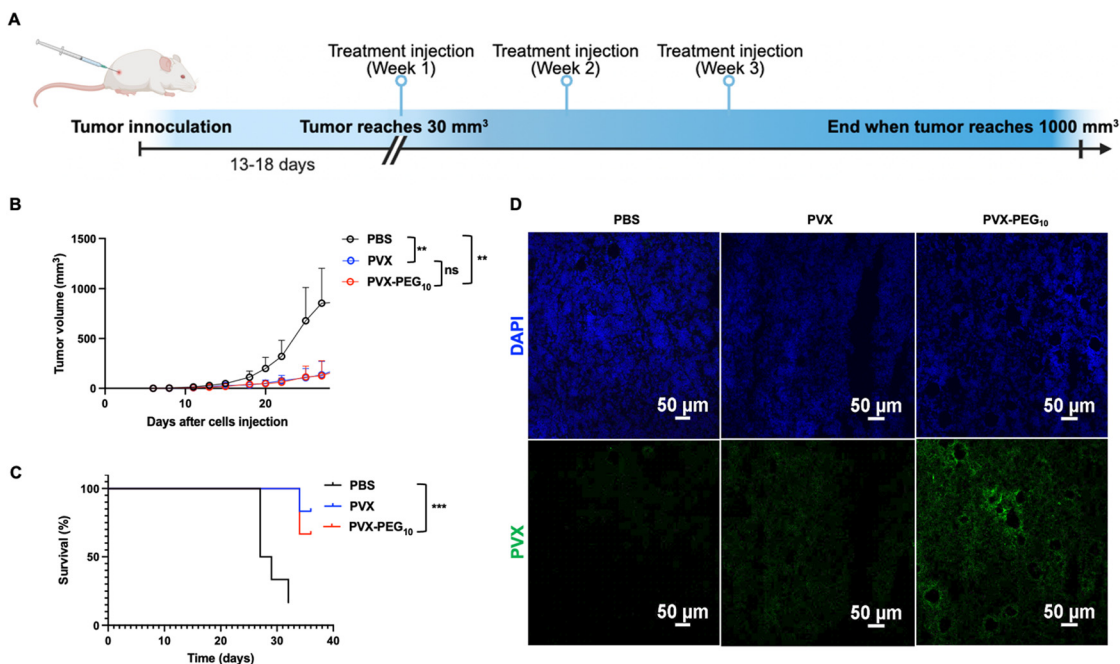


Fig. 2 Anti-tumor efficacy of PVX and PVX-PEG₁₀ against A20 lymphoma using BALB/C mice. (A) Treatment schedule. (B) Tumor growth curve and (C) survival data were plotted for each group (** $p < 0.01$, *** $p < 0.001$). (D) Confocal microscopy of tumor sections collected 24 h post first treatment dose; stained for DAPI and PVX.

($n = 5$ per group); three weekly injections at 0.1 mg dose were administered by intratumoral administration (Fig. 2). As reported in our previous study, PVX demonstrated potent anti-tumor efficacy resulting in tumor growth control and prolonged survival (Fig. 2B and C). This data was matched using PVX-PEG indicating that crosslinking or PEGylation does not impair the anti-tumor efficacy of PVX.

In our previous study we noted that PVX was rapidly cleared from the TME and not detectable 72 hours post administration – this is in stark contrast to CPMV which persists within the TME.¹¹ We wondered whether the stabilized crosslinked PVX-PEG would have increased tissue residence and therefore collected A20 tumors 24 hours post one administration of PVX

or PVX-PEG and imaged PVX by staining with an α -PVX antibody and confocal microscopy. Indeed, data indicate increased presence of PVX-PEG within the TME 24 hours post treatment (Fig. 2D). Further research is required to investigate whether this increased retention impacts the anti-tumor efficacy or whether PEGylation changes the intratumoral cell uptake and innate immune cell activation. However, we hypothesize that prolonged TME residence time is beneficial for longitudinal immune signaling and activation of the cancer immunity cycle.

Antibody recognition of PVX-PEG is reduced

Finally, we investigated whether the PVX-PEG₁₀ formulation conferred reduced antibody recognition. For this, we produced

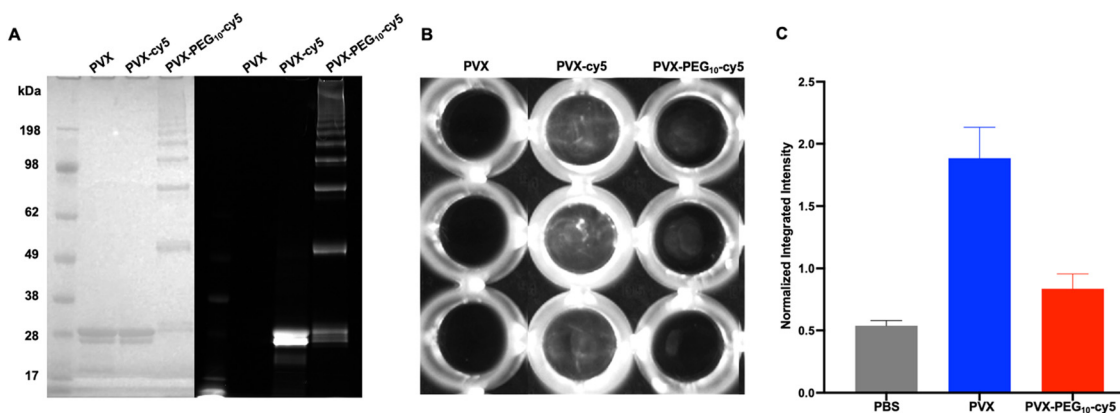


Fig. 3 PEGylation reduced antibody recognition of PVX-PEG. (A) SDS-PAGE of PVX and Cy5-labeled PVX and crosslinked PVX-PEG₁₀ imaged after Coomassie staining and under white light (left) and using a red fluorescence channel confirming conjugation of the Cy5 dye. (B) Antibody recognition sandwich assay (in triplicate) to detect binding of cy5-labeled PVX or crosslinked PVX-PEG_n to an α -PVX coated plate. Imaging data in (B) and quantitative data in (C).



fluorescently-labeled PVX and PVX-PEG₁₀ by targeting solvent-exposed Cys side chains. Fewer than 10 Cy5 labels were introduced per PVX or PVX-PEG₁₀ and the fluorescence intensity of the samples was comparable; covalent conjugation was verified by SDS-PAGE (Fig. 3A). Polyclonal α -PVX antibodies from rabbits were coated on 96-well plates and binding of PVX vs. PVX-PEG₁₀ was tested by adding the samples to the wells. This format was chosen to maintain the structure of PVX and PVX-PEG₁₀, and to avoid protein and polymer spreading which can be observed when the virus nanoparticle samples are immobilized on the plates instead. Imaging of the plates and quantitative analysis with Fiji ImageJ showed that the PVX-PEG₁₀ has significantly reduced binding to the plates indicating that the PEG coating forms an effective stealth coating to reduce immune recognition. From a translational point of view this may be important, because plant viruses are prevalent, and several reports indicate human exposure and pre-existing immunity against various plant viruses.^{16,17,23}

Conclusions

Our study demonstrates the feasibility and efficacy of PEGylated potato virus X (PVX-PEG_n) as an intratumoral immunotherapy for B-cell lymphoma. We successfully synthesized and characterized PVX-PEG, showing that PEGylation enhances the formulation's stability while maintaining its immunostimulatory and anti-tumor properties. Importantly, PVX-PEG exhibited prolonged retention in the tumor micro-environment, suggesting potential benefits for sustained immune activation. Furthermore, PEGylation reduced antibody recognition, which may improve translational prospects by mitigating concerns regarding pre-existing immunity and off-target effects. In our previous work, we demonstrated that localized treatment of a single cancerous lesion using plant viruses, including PVX, can induce potent systemic anti-tumor immunity leading to abscopal effect and long-lasting immune memory.^{8,11,24} While further research using PVX-PEG in this context is needed, we establish this formulation as a promising candidate for further validation and potential future clinical translation in intratumoral immunotherapy.

Materials & methods

Materials

All materials were bought from Thermo Fisher Scientific unless stated otherwise. PVX was purified from *N. benthamiana* plants as previously described.²⁵ Native and PEGylated PVX were diluted with 0.1 M potassium phosphate buffer pH 7.0 buffer (denoted as KP buffer) unless stated otherwise. Native PVX, PEGylated PVX, and reaction intermediates were stored at 4 °C in 0.1 M KP unless stated otherwise.

Synthesis of PVX-PEG

Linear bis-PEG_n-NHS esters (PEG₁₀, PEG₁₈, and PEG₂₅) were prepared as stock solutions at 100 mg mL⁻¹ in DMSO and

added dropwise to PVX in KP buffer with a final ratio of CP to PEG of 1 : 1, 1 : 5, 1 : 10, 1 : 15 and 1 : 18. The final concentration of PVX was adjusted to 2 mg mL⁻¹ in KP buffer and a final DMSO concentration of 10% by volume. The reaction mixture was incubated overnight at 4 °C and purified by ultracentrifugation at 50 000g for 1 h on a 30% (w/v) sucrose cushion. The purified crosslinked PVX was resuspended in KP buffer.

PVX concentration measurement

Particle concentration was determined using either UV-Vis spectroscopy or the Pierce™ BCA Protein Assay Kit. Absorbance at 260 nm and 280 nm was measured using a NanoDrop spectrophotometer. The Beer-Lambert law and the extinction coefficient of PVX at 260 nm (2.97 mL mg⁻¹ cm⁻¹) were applied to the absorbance measurements to calculate the concentration. The Pierce™ BCA Protein Assay Kit was used according to the manufacturer's instructions and read with the NanoDrop spectrophotometer.

Sodium dodecyl sulfate-polyacrylamide gel electrophoresis (SDS-PAGE)

PVX and PVX-PEG (5 μg) were heated at 95 °C for 5 minutes with NuPAGE™ LDS Sample Buffer (4X) (Invitrogen). The denatured samples were loaded onto precast 4–12% NuPAGE™ Bis-Tris gels (Invitrogen) and electrophoresed at 200 V, 120 mA, and 25 W using 1X MOPS SDS running buffer (Invitrogen). SeeBlue™ Plus2 Pre-stained Protein Standard (Invitrogen) was loaded in a separate lane on each gel for molecular weight estimation. Gels were removed from the casts, stained with Coomassie Brilliant Blue R-250 (Thermo Fisher Scientific), and imaged with an AlphaImager (ProteinSimple). Conjugation rates were analyzed with ImageJ.

Dynamic light scattering (DLS)

PVX, PVX-PEG₁₀, PVX-PEG₁₈, and PVX-PEG₂₅ (10 μL, 0.1 mg mL⁻¹) were run on a Zetasizer Nano ZSP/Zen5600 (Malvern Panalytical) at 25 °C.

Transmission electron microscopy

PVX and PVX-PEG₁₀ (10 μL, 0.1 mg mL⁻¹) were diluted in ultrapure water and applied onto easiGlow (PELCO) glow-discharged formvar-coated grids (Electron Microscopy Sciences). The grids were washed twice with 10 μL ultrapure water (Invitrogen) for 45 seconds each time and stained twice with 10 μL of 2% (w/v) uranyl acetate for 35 seconds each time. TEM images were acquired using a JEOL 1400 Plus.

Formulation stability assays

For thermal stability assays PVX and PVX-PEG were used at 1 mg mL⁻¹ in KP buffer. PVX and PVX-PEG samples were incubated at 25 °C, 37 °C, 60 °C, 70 °C, and 80 °C – the temperature was ramped from 25 °C to 80 °C within a period of 15 min using a PCR thermocycler. Samples were cooled down to room temperature and then transferred to a clear bottom 96-well plate and absorbance at 600 nm was measured using a



Tecan plate reader. Samples incubated at different temperatures were also subjected to DLS measurements.

For stability assessment under biological conditions, blood was collected from female BALB/c mice (Jackson Laboratory) with lithium-heparin treated tubes by retro-orbital bleeding. Mouse plasma was extracted by centrifugation the blood at 20 000g for 10 min at 4 °C. PVX and PVX-PEG (1 mg mL⁻¹) were then incubated in 50% (v/v) mouse plasma in KP buffer for 24 hours at 37 °C. Samples were then visually inspected for aggregation.

A20 tumor mouse model

A20 B cell lymphoma cells (ATCC) were cultured in RPMI-1640 medium, supplemented with 10% (v/v) fetal bovine serum (FBS) (Gibco), 1% (v/v) penicillin–streptomycin (10 000 U mL⁻¹) (Gibco), and 0.05 mM 2-mercaptoethanol, at 37 °C under 5% CO₂. A20 cells were passaged as per ATCC's instruction.

Animal protocols were approved by University of California San Diego's Institutional Animal Care and Use Committee. Female BALB/c mice (7–8 weeks old) were purchased from Jackson Laboratory. To establish A20 dermal tumors, 2 × 10⁵ cells in 30 μL PBS was inoculated intradermally into the right flank of a BALB/c mouse. 100 μg PVX or PVX-PEG₁₀ in 20 μL sterile PBS or 20 μL PBS for the control group was injected intratumorally weekly for 3 times after the tumor volume reaches 30 mm³. The mice were monitored three times every week for tumor growth. The tumor size was measured as:

$V = \frac{L \times W^2}{2}$, where V is tumor volume, L is tumor length, and W is tumor width ($L > W$). Mice were sacrificed when the tumor reached 1000 mm³. Microsoft Excel and GraphPad Prism 9 were used to run statistical tests and plot data.

Significances were determined by two-way analysis of variance with Tukey's multiple comparisons test in GraphPad Prism 9. Survival data were compared with Mantel-Cox test in GraphPad Prism 9.

Confocal microscopy

Mice were inoculated with A20 cells and treated as described above. 24 hours post first intratumoral treatment, the tumors were harvested, flash frozen in liquid nitrogen, embedded in OCT medium, and then cut into 10 μm-thin sections using a Leica microsystem CM1860 cryostat; the slides were then mounted onto Superfrost Plus microscope slides. The sections were washed in PBS for 5 min and fixed with 4% (v/v) paraformaldehyde in PBS for 10 min. After 3 washes in PBS (5 min/time), the slides were blocked with 1% (w/v) bovine serum albumin (BSA) in PBS with 0.1% (v/v) Tween-20 (PBST) for 1 hour at room temperature and then washed 3 times using PBST. The slides were incubated using 1 μg mL⁻¹ rabbit α-PVX (Pacific Immunology) in PBST with 1% (w/v) BSA for 1 hour at room temperature in the dark. After 3 washes, the slides were incubated in 1:1000 diluted Alexa Fluor 488 goat anti-rabbit IgG (Invitrogen Cat# A-11008) in PBST with 1% (w/v) BSA for 1 hour at room temperature in the dark and washed 3 times using PBST. The slides were mounted with fluoroshield

containing DAPI (Sigma Aldrich) for 10 min at room temperature and sealed with a coverslip and nail polish. The slides were viewed with a Nikon A1R confocal/TIRF STORM confocal microscopy.

Fluorescent Cy5-labeled PVX and PVX-PEG

Cystine residues of the PVX or PVX-PEG (at 2 mg mL⁻¹ in KP buffer) was conjugated with Cy5-maleimide using a ratio of coat protein and Cy5 of 1:10; Cy5; Cy5 was added in DMSO and the final DMSO concentration was adjusted to 10% by volume. Excess Cy5 was removed by ultracentrifugation at 50 000g for 1 hour at 4 °C; Cy5-labeled PVX and PVX-PEG were resuspended in KP buffer and the number of dyes per particle was determined by UV/vis measurement using the PVX and Cy5-specific extinction coefficients and Beer-Lambert law.

Antibody recognition assay

A 96-well plate was coated with 100 μL (1 μg mL⁻¹) rabbit α-PVX and incubated overnight at 4 °C. The plate was washed 3 times using 200 μL PBS-T. Blocking was achieved using 100 μL of 3% (w/v) BSA in PBS-T and incubation for 1 hour at 37 °C. The plates were washed again 3 times with PBS-T. Then 10 μg PVX, PVX-cy5, and PVX-PEG₁₀-cy5 in 100 μL KP buffer were added and incubated for 1 hour at 37 °C (in triplactes). The plate was washed 3 times with PBS-T and imaged with a Bio-Rad GelDoc at cy5 channel. The intensity was measured with Fiji ImageJ software (<https://imagej.net/software/fiji/>).

Conflicts of interest

N. F. S. declares the following competing financial interest(s): Dr Steinmetz is a co-founder and CEO of and has equity in PlantiosX Inc. Dr Steinmetz is a co-founder of and has equity in Mosaic ImmunoEngineering Inc. Dr Steinmetz is a co-founder and manager of Pokometz Scientific LLC, under which she is a paid consultant to Flagship Labs 95 Inc. The other authors do not have any COIs.

Data availability

Data is available from the authors upon reasonable request.

Acknowledgements

This work was supported partially by the National Science Foundation through the University of California San Diego Materials Research Science and Engineering Center (UCSD MRSEC), grant number DMR-2011924. This work was supported in part at the San Diego Nanotechnology Infrastructure (SDNI) of University of California San Diego, a member of the National Nanotechnology Coordinated Infrastructure (NNCI), which is supported by the National Science Foundation (Grant ECCS-1542148). The *in vivo* work was supported in part through NIH Grants R01 CA224605 and R01 CA274640 (to N. F. S.).



References

- 1 P. S. Hegde and D. S. Chen, Top 10 Challenges in Cancer Immunotherapy, *Immunity*, 2020, **52**(1), 17–35.
- 2 O. Hamid, R. Ismail and I. Puzanov, Intratumoral Immunotherapy-Update 2019, *Oncologist*, 2020, **25**(3), e423–e438.
- 3 M. Ghosn, L. Tselikas, S. Champiat, F. Deschamps, B. Bonnet, E. Carre, M. Testan, F. X. Danlos, S. Farhane, S. Susini, S. Suzzoni, S. Ammari, A. Marabelle and T. De Baere, Intratumoral Immunotherapy: Is It Ready for Prime Time?, *Curr. Oncol. Rep.*, 2023, **25**(8), 857–867.
- 4 C. R. Shyr, L. C. Liu, H. S. Chien and C. P. Huang, Immunotherapeutic Agents for Intratumoral Immunotherapy, *Vaccines*, 2023, **11**(11), 1717.
- 5 C. Mao, V. Beiss, J. Fields, N. F. Steinmetz and S. Fiering, Cowpea mosaic virus stimulates antitumor immunity through recognition by multiple MYD88-dependent toll-like receptors, *Biomaterials*, 2021, **275**, 120914.
- 6 J. Jobsri, A. Allen, D. Rajagopal, M. Shipton, K. Kanyuka, G. P. Lomonosoff, C. Ottensmeier, S. S. Diebold, F. K. Stevenson and N. Savelyeva, Plant virus particles carrying tumour antigen activate TLR7 and Induce high levels of protective antibody, *PLoS One*, 2015, **10**(2), e0118096.
- 7 V. Beiss, C. Mao, S. N. Fiering and N. F. Steinmetz, Cowpea Mosaic Virus Outperforms Other Members of the Secoviridae as In Situ Vaccine for Cancer Immunotherapy, *Mol. Pharm.*, 2022, **19**(5), 1573–1585.
- 8 D. Alonso-Miguel, G. Valdivia, D. Guerrero, M. D. Perez-Alenza, S. Pantelyushin, A. Alonso-Diez, V. Beiss, S. Fiering, N. F. Steinmetz, M. Suarez-Redondo, Jv Berg, L. Peña and H. Arias-Pulido, Neoadjuvant in situ vaccination with cowpea mosaic virus as a novel therapy against canine inflammatory mammary cancer, *J. Immunother. Cancer*, 2022, **10**(3), e004044.
- 9 S. Shukla, C. Wang, V. Beiss, H. Cai, T. Washington, 2nd, A. A. Murray, X. Gong, Z. Zhao, H. Masarapu, A. Zlotnick, S. Fiering and N. F. Steinmetz, The unique potency of Cowpea mosaic virus (CPMV) in situ cancer vaccine, *Biomater. Sci.*, 2020, **8**(19), 5489–5503.
- 10 M. E. Lebel, K. Chartrand, E. Tarrab, P. Savard, D. Leclerc and A. Lamarre, Potentiating Cancer Immunotherapy Using Papaya Mosaic Virus-Derived Nanoparticles, *Nano Lett.*, 2016, **16**(3), 1826–1832.
- 11 J. F. Affonso de Oliveira, M. A. Moreno-Gonzalez, Y. Ma, X. Deng, J. Schuphan and N. F. Steinmetz, Plant Virus Intratumoral Immunotherapy with CPMV and PVX Elicits Durable Antitumor Immunity in a Mouse Model of Diffuse Large B-Cell Lymphoma, *Mol. Pharm.*, 2024, **21**(12), 6206–6219.
- 12 M. J. Frank, P. M. Reagan, N. L. Bartlett, L. I. Gordon, J. W. Friedberg, D. K. Czerwinski, S. R. Long, R. T. Hoppe, R. Janssen, A. F. Candia, R. L. Coffman and R. Levy, In Situ Vaccination with a TLR9 Agonist and Local Low-Dose Radiation Induces Systemic Responses in Untreated Indolent Lymphoma, *Cancer Discovery*, 2018, **8**(10), 1258–1269.
- 13 L. Hammerich, T. U. Marron, R. Upadhyay, J. Svensson-Arvelund, M. Dhainaut, S. Hussein, Y. Zhan, D. Ostrowski, M. Yellin, H. Marsh, A. M. Salazar, A. H. Rahman, B. D. Brown, M. Merad and J. D. Brody, Systemic clinical tumor regressions and potentiation of PD1 blockade with in situ vaccination, *Nat. Med.*, 2019, **25**(5), 814–824.
- 14 J. D. Brody, W. Z. Ai, D. K. Czerwinski, J. A. Torchia, M. Levy, R. H. Advani, Y. H. Kim, R. T. Hoppe, S. J. Knox, L. K. Shin, I. Wapnir, R. J. Tibshirani and R. Levy, In situ vaccination with a TLR9 agonist induces systemic lymphoma regression: a phase I/II study, *J. Clin. Oncol.*, 2010, **28**(28), 4324–4332.
- 15 M. A. Nemykh, V. K. Novikov, A. M. Arutiunian, P. V. Kalmykov, V. A. Drachev and E. N. Dobrov, [Comparative study of structural stability of potato virus X coat protein molecules in solution and in the virus particles], *Mol. Biol.*, 2007, **41**(4), 697–705.
- 16 Y. Aguado-Garcia, B. Taboada, P. Moran, X. Rivera-Gutierrez, A. Serrano-Vazquez, P. Isa, L. Rojas-Velazquez, H. Perez-Juarez, S. Lopez, J. Torres, C. Ximenez and C. F. Arias, Tobamoviruses can be frequently present in the oropharynx and gut of infants during their first year of life, *Sci. Rep.*, 2020, **10**(1), 13595.
- 17 J. F. Affonso de Oliveira, S. K. Chan, A. O. Omole, V. Agrawal and N. F. Steinmetz, In Vivo Fate of Cowpea Mosaic Virus In Situ Vaccine: Biodistribution and Clearance, *ACS Nano*, 2022, **16**(11), 18315–18328.
- 18 S. Saxena, S. Sharma, G. Kumar and S. Thakur, Unravelling the complexity of CARPA: a review of emerging advancements in therapeutic strategies, *Arch. Dermatol. Res.*, 2025, **317**, 439.
- 19 J. M. Harris and R. B. Chess, Effect of pegylation on pharmaceuticals, *Nat. Rev. Drug Discovery*, 2003, **2**(3), 214–221.
- 20 K. L. Lee, S. Shukla, M. Wu, N. R. Ayat, C. E. El Sanadi, A. M. Wen, J. F. Edelbrock, J. K. Pokorski, U. Commandeur, G. R. Dubyak and N. F. Steinmetz, Stealth filaments: Polymer chain length and conformation affect the in vivo fate of PEGylated potato virus X, *Acta Biomater.*, 2015, **19**, 166–179.
- 21 D. H. T. Le, H. Hu, U. Commandeur and N. F. Steinmetz, Chemical addressability of potato virus X for its applications in bio/nanotechnology, *J. Struct. Biol.*, 2017, **200**(3), 360–368.
- 22 Z. Wu, L. J. Bayón, T. B. Kouznetsova, T. Ouchi, K. J. Barkovich, S. K. Hsu, S. L. Craig and N. F. Steinmetz, Virus-like particles armored by an endoskeleton, *Nano Lett.*, 2024, **24**(10), 2989–2997.
- 23 R. Liu, R. A. Vaishnav, A. M. Roberts and R. P. Friedland, Humans have antibodies against a plant virus: evidence from tobacco mosaic virus, *PLoS One*, 2013, **8**(4), e60621.
- 24 C. Mao, V. Beiss, G. W. Ho, J. Fields, N. F. Steinmetz and S. Fiering, In situ vaccination with cowpea mosaic virus elicits systemic antitumor immunity and potentiates immune checkpoint blockade, *J. Immunother. Cancer*, 2022, **10**(12), e005834.
- 25 K. L. Lee, K. Uhde-Holzem, R. Fischer, U. Commandeur and N. F. Steinmetz, Genetic engineering and chemical modification of potato virus X, *Methods Mol. Biol.*, 2014, **1108**, 3–21.

